 doi:10.20944/preprints201907.0113.v1

Article

On the determining role of texture in causing delamination during impact fracture of Ti and Nb-Ti microalloyed steel

Mingyu Sun [1], Xuemin Wang [1,*] and R.D.K. Misra [2]

[1] Collaborative Innovation Center of Steel Technology, University of Science and Technology Beijing, No.30, Xueyuan Road, Haidian District, Beijing, 10083, China; sunmingyudi@163.com (M.Y. S.)

[2] Laboratory for Excellence in Advanced Steel Research, Materials Science and Engineering Program, Department of Metallurgical, Materials and Biomedical Engineering, University of Texas at El Paso, 500 W. University Avenue, El Paso, TX 79968, USA; dmisra2@utep.edu (R.D.K. Misra)

* Correspondence: wxm@mater.ustb.edu.cn; Tel.: +86-010-6233-4910

Abstract: 700 MPa grade Ti and Nb-Ti microalloyed steels produced by thermo-mechanical control rolled processes (TMCP) were studied to elucidate texture that contributes to delamination and consequent impact toughness. The microstructure of Ti and Nb-Ti steels consisted of ferrite and bainite. Compared with Ti steel, Nb-Ti steel was characterized by a microstructure with finer ferrite and more bainite. The results from tensile and impact tests indicated that there is insignificant change in tensile properties, but toughness was greater in Nb-Ti steel compared with Ti steel. More severe delamination in Nb-Ti steel is attributed to stronger α-fiber (RD ||<110>) texture than Ti steel, especially {100}<110>, {113}<110> and {112}<110> texture. Typical cleavage river patterns were not observed on delaminated fracture surface, instead the cleavage fracture surface indicated some dimples. Interestingly, the impact energy of samples with delamination was greater than samples without delamination in the ductile–brittle transition region. The study suggests that delamination in the ductile–brittle transition zone may also be representative of high toughness.

Keywords: Ti and Nb-Ti microalloyed steel, microstructure, toughness, texture, delamination

1. Introduction

High strength and high toughness steels are required in high strength low alloy (HSLA) steels to reduce weight and ensure safety [1]. Grain refinement is the most effective and economical approach to improve strength and toughness, which can be achieved by the thermo-mechanical control rolled processes (TMCP) [2]. Rolling in the austenite non-recrystallization region is an effective way to improve grain refinement. By retarding recrystallization, strain can be accumulated and the microstructure can be refined after phase transformation [3]. Furthermore, TMCP tends to develop strong fiber texture and results in anisotropy in microstructure and mechanical properties. The bcc transformation products have a crystallographic texture which is related to the texture of parent austenite (γ). A fairly sharp rolling texture can be produced in γ by introducing sufficient strain in the austenite non-recrystallization region, which translates into a sharp texture in α-products [4]. However, previous studies showed that HSLA steels produced by TMCP display marked anisotropy in toughness and cause fracture delamination [5]. The effect of delamination on impact toughness has been previously studied in HSLA steels [6-9]. It is reported that delamination reduced the notch impact toughness in the upper shelf region [7,8,10]. On the other hand, other studies showed that delamination can improve toughness [11,12]. Furthermore, the initiation of delamination fracture in Charpy impact test has not yet been sufficiently explained. It was reported that the delamination fracture of Charpy impact samples was caused by many factors, such as ferrite-pearlite

Preprints (www.preprints.org) | NOT PEER-REVIEWED | Posted: 8 July 2019 doi:10.20944/preprints201907.0113.v1

microstructure [13], elongated grains [14], certain texture characteristics [15], aligned particles [16], and inclusions banding [17].

HSLA steels produced by TMCP exhibit strong anisotropy due to strain accumulation introduced during rolling in the austenite non-recrystallization region. It is well known that niobium is an effective microalloying element that retards austenite recrystallization because of solute drag effect of Nb and the pinning effect of fine precipitates such as NbC, which is beneficial for accumulating sufficient strain during TMCP [18]. Although many studies discussed the effect of TMCP on microstructural and textural evolution in HSLA steel [19-21], there are only few studies on the effect of Nb on the texture evolution in HSLA steel produced by TMCP [22]. In addition, delamination is usually associated with strong texture, which has an influence on toughness.

Thus, based on the above discussion, Ti and Nb-Ti microallyed steels produced by TMCP were studied to elucidate the nature of texture that contribute to delamination and consequent toughness.

2. Materials and Methods

The present study was carried out on 700 MPa Ti and Nb-Ti microalloyed steels with thickness of 10 mm. The experimental steels manufactured through thermal mechanical control processing (TMCP). The rolling schedules are almost same for two steels. The steels were rolled via a series of passes between 1050 – 960 °C and 890 – 850 °C, and the plates were coiled at 600 °C. The chemical composition of the experimental steels is given in Table 1. Because of the cheaper price of the Ti-Fe than other alloying elements, high Ti content is designed in experimental steels to lower the cost while increasing strength by precipitation strenthening. The Ti microalloyed steel without Nb was used for comparison with Nb-Ti microalloyed steel.

Table 1. Chemical composition of the material (wt.%)

steels	C	Si	Mn	Nb	Ti	N	P	S
Ti	0.08	0.12	1.6	---	0.09	0.0045	0.010	0.002
Nb-Ti	0.07	0.1	1.5	0.04	0.08	0.0040	0.012	0.002

Tensile and Charpy specimens were cut from the experimental steels from the longitudinal direction. Tensile tests were conducted via WDW-200D material testing machine at a constant crosshead speed of 3 mm/min. Standard CVN specimens of dimensions 55 mm×10 mm×7.5 mm were machined and tested at 0 °C, -20 °C, -40 °C, -60 °C and -80 °C.

For optical microscopy (OM) and scanning electron microscopy (SEM), the samples were etched with 4% nital after mechanical polishing. Transmission electron microscopy (TEM) foils were twin-jet electropolished to perforation using a solution of 5% perchloric acid and 95% ethanol at -20 °C after mechanically thinning to 50 μm. JEOL JEM-2100 TEM operated at 200 keV was used for examining the foils.

Macrotexture measurements were performed on a D8 Advance X-Ray diffractometer. Texture measurements were made from an area of 25×20 mm. (110), (200) and (211) pole figures were used to construct orientation distribution functions (ODFs) in three-dimensional Euler space using Tex Eval software. All samples for macrotexture measurements were selected from the mid-thickness of the steels close to the mid-position.

3. Results and Discussion

3.1. Microstructure

Figure 1 shows OM and SEM micrographs of the studied steels. It can be seen from Figure 1a,b that the main microstructure of Ti and Nb-Ti microalloyed steels is ferrite and bainite. High

Preprints (www.preprints.org) | NOT PEER-REVIEWED | Posted: 8 July 2019 doi:10.20944/preprints201907.0113.v1

magnification of microstructure obtained by using SEM is shown in Figure 1c,d. It can be seen that the representative microstructure of Ti and Nb-Ti steels consisted of ferrite and bainite. Compared to Ti steel, Nb-Ti steel displays a microstructure with finer ferrite and more bainite, attributing to the effect of Nb in delaying ferrite transformation. The results show that the addition of Nb in microalloyed steel can decrease ferrite content and refine grain size, which can be attributed to the role of Nb in delaying ferrite transformation.

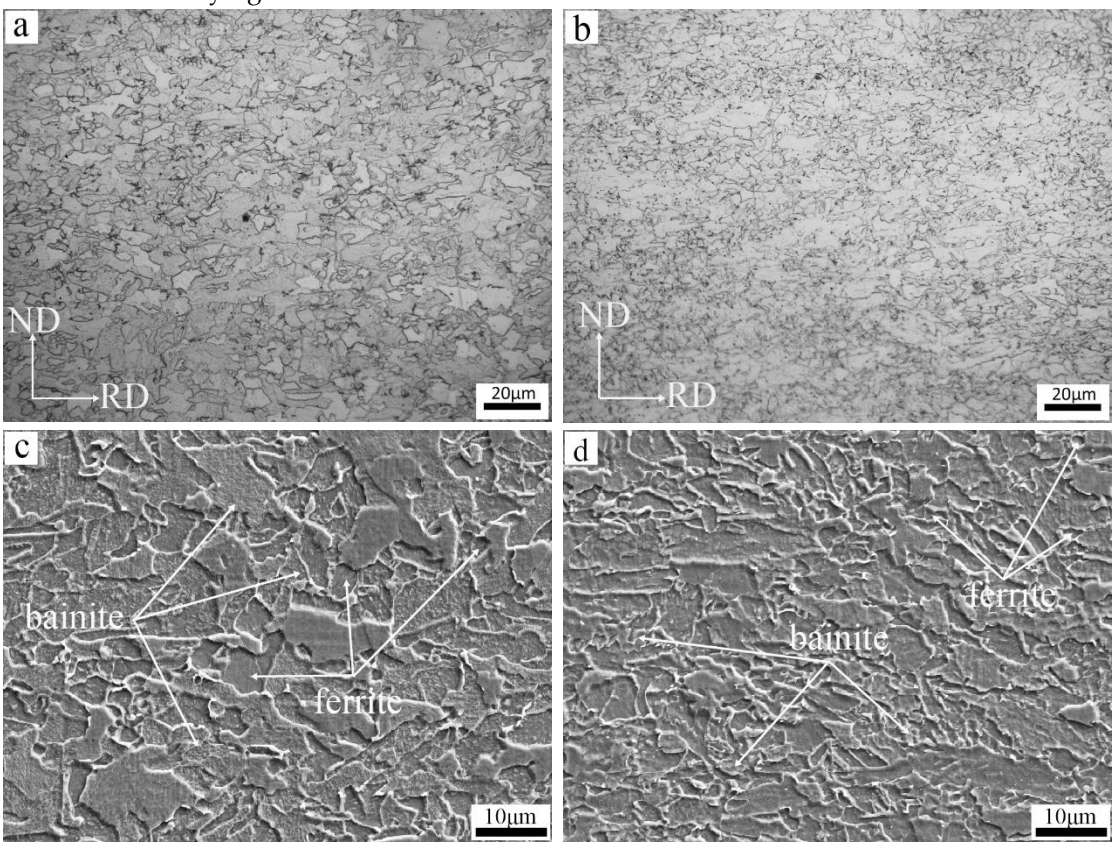

Figure 1. OM and SEM micrographs of experimental steels (**a**) (**c**) Ti steel, (**b**) (**d**) Nb-Ti steel.

Fine precipitates with size of less than 10 nm were obtained in ferrite, as shown in Figure 2. It can be seen that there is a large amount of fine precipitates, especially interphase precipitates in both two steels. The interphase precipitation occurs during γ/α phase transformation and the coiling process at 600 °C increases the amount of interphase precipitates. As the size is too small, their composition could not be measured quantitatively by EDS. However, based on their shape, size and the chemical composition of the experimental steels, these precipitates were speculated to be TiC or (Ti,Nb)C [23].

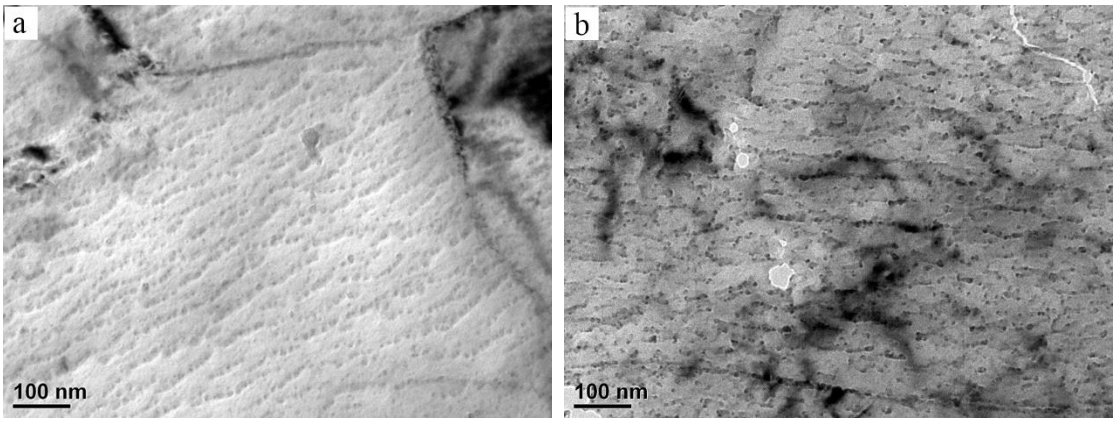

Preprints (www.preprints.org) | NOT PEER-REVIEWED | Posted: 8 July 2019 doi:10.20944/preprints201907.0113.v1

Figure 2. B TEM micrographs of fine precipitates in experimental steels (**a**) Ti steel, (**b**) Nb-Ti steel.

3.1. Mechanical properties

Tensile properties of steels are given in Table 2. Compared with Ti steel, the strength and elongation of Nb-Ti steel was higher. The results of CVN impact energy vs. temperature and the ductile–brittle transition temperature (DBTT) is shown in Figure 3. A sharp drop in absorbed energy occurred in Ti steel when temperature decreased from 0 °C to −20 °C, which is caused by the occurrence of brittle fracture. With further decrease in temperature, the absorbed energy reduced rapidly. In Nb-Ti steel, the absorbed energy reduced gradually with decrease in temperature from 0 °C to −40 °C and a sharp drop in absorbed energy occurred at -60 °C. It can be seen from Figure 3 that the impact toughness of Nb-Ti steel was significantly higher than Ti steel. Moreover, the DBTT of Nb-Ti steel was ~ -60 °C, which was lower than Ti steel (~ -20 °C).

Table 2. Mechanical properties of experimental steels

steels	R_{eL}/MPa	R_m/MPa	A_{25}/%
Ti	723	769	19.5
Nb-Ti	732	781	20.5

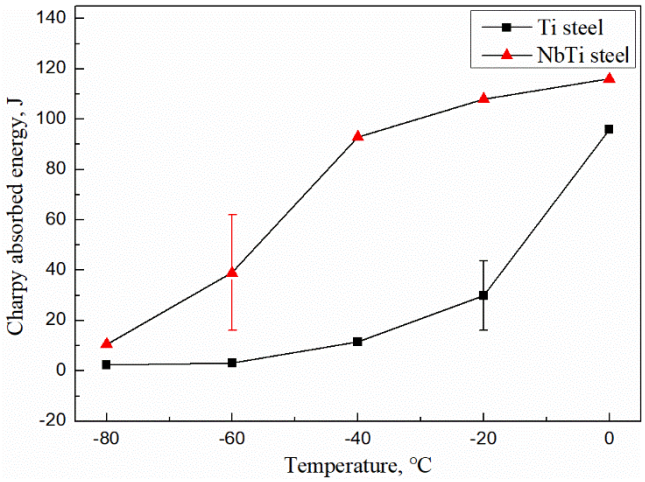

Figure 3. Charpy V-notch impact energy vs. temperature and the DBTT of experimental steels.

3.3. Fracture surfaces

To study the effect of delamination on impact toughness, the morphology of the fracture samples was examined by SEM, as shown in Figures 4 and 5. Figure 4a shows SEM micrographs of Nb-Ti samples after Charpy impact test at temperatures of 0 °C, -20 °C, -40 °C and -80 °C, respectively. The fracture mode of Nb-Ti samples varied gradually from fully ductile to brittle fracture with decreasing temperature, consistent with Charpy impact toughness as a function of temperature. Fracture surface of Nb-Ti samples tested at 0 °C, -20 °C and -40 °C were characterized by both ductile and delamination features, while the dominant brittle fracture without delamination existed at -80 °C.

Preprints (www.preprints.org) | NOT PEER-REVIEWED | Posted: 8 July 2019 doi:10.20944/preprints201907.0113.v1

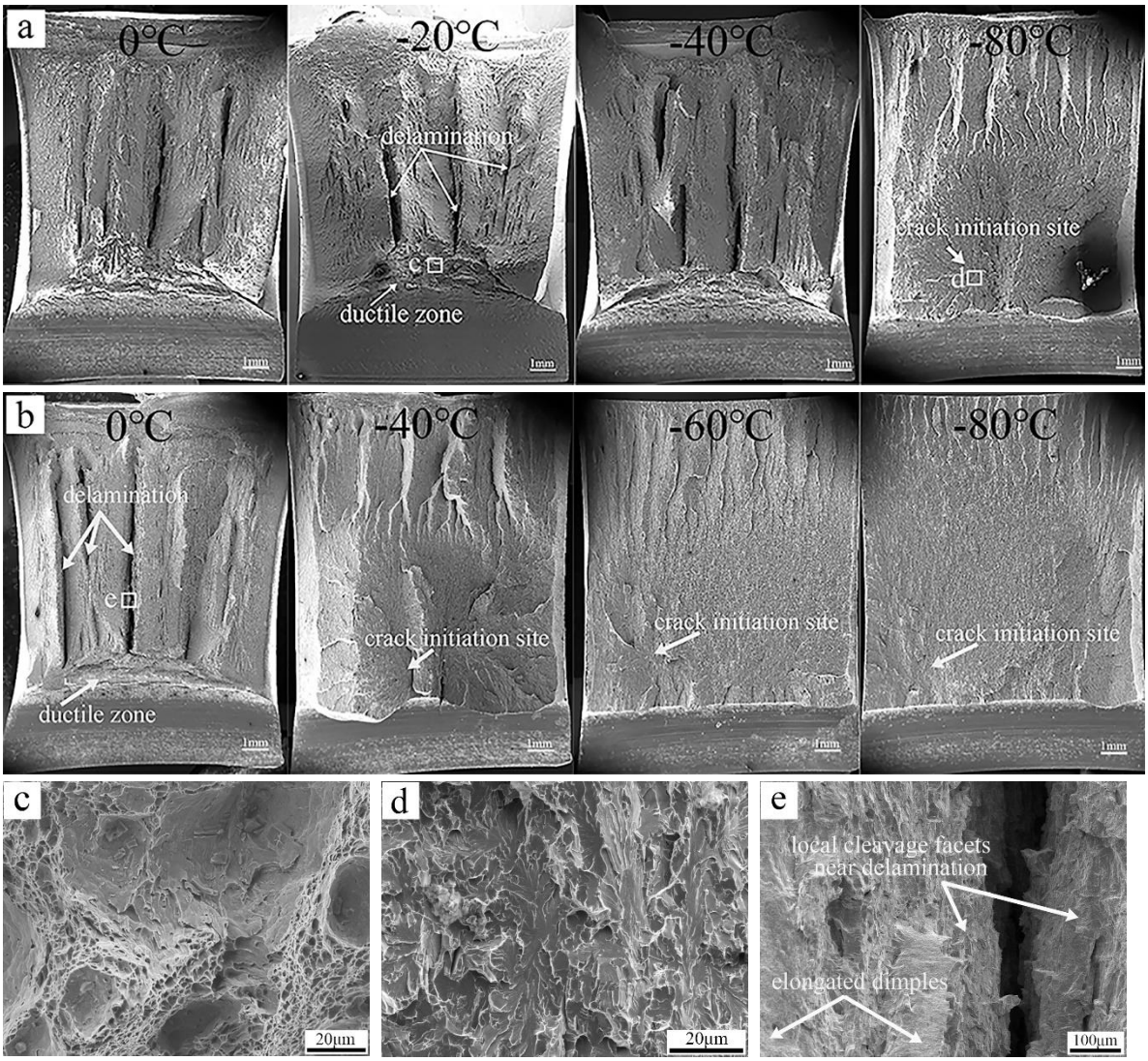

Figure 4. Fracture surface of Charpy impact samples tested at different temperatures (**a**) (**b**) SEM micrographs of fracture surface of Nb-Ti steel and Ti steel at different test temperatures, respectively, (**c**) (**d**) the magnified SEM micrographs of the selected areas marked by 'c', and 'd' in (a), respectively, (**e**) the magnified SEM micrographs of the selected areas marked by 'e' in (b).

The fracture near the notch-root for the Nb-Ti sample tested at -20 °C was found to be ductile in nature, with large distribution of dimples as shown in Figure 4c. In the upper shelf region, fracture occurred by nucleation and coalescence of microvoids involving ductile tearing, which requires extensive plastic deformation. The wider ductile zone means greater degree of plastic deformation was experienced by the sample during impact test. The Nb-Ti sample tested at -80 °C experienced almost no plastic deformation with a corresponding minimum value of impact energy of 10.5 J, as shown in Figures 3 and 4a. It can be seen from Figure 4d that cleavage fracture was dominant without delamination in Nb-Ti sample tested at -80 °C. For Ti steel, the ductile fracture with delamination occurred at -0 °C, while the cleavage fracture without delamination occurred at -40 °C, -60 °C and -80 °C, as shown in Figure 4b. Although the dominant ductile fracture existed in the upper shelf region, the corresponding impact energy of specimen was not very high due to the presence of local cleavage facets near delamination as shown in Figures 3 and 4e. Delamination in the ductile fracture regime normally reduces the upper shelf energy and is generally associated with the separation of {001} cleavage planes [7,12]. Grain with {001} planes parallel to the rolling plane greatly reduce the local

Preprints (www.preprints.org) | NOT PEER-REVIEWED | Posted: 8 July 2019 doi:10.20944/preprints201907.0113.v1

cleavage fracture stress on these planes, leading to a cleavage behavior parallel to the rolling plane during the impact process, since {001} planes promote cleavage fracture in bcc metals. This cleavage behavior is likely to form deep groove shape cleavage cracks which were responsible for the decrease in the impact energy, even though the steel was 100% ductile in the upper shelf region [24].

Figure 5 shows SEM micrographs of Nb-Ti and Ti samples after Charpy impact test at the DBTT of -60 °C and -20 °C, respectively. Three impact samples were compared for each of Ti and Nb-Ti steels to better understand the effect of delamination on toughness in the ductile–brittle transition region. Figure 5a shows that Nb1, Nb2 and Nb3 samples with impact energy of 62J, 39J, 16J, respectively, while Figure 5b shows Ti1, Ti2 and Ti3 samples with impact energy of 45J, 18J, 26J, respectively. The fracture near the notch-root for Nb1 and Ti1 samples were found to be ductile with prominent dimples, as shown in Figure 5c,f. At the center of the Nb1 sample, the mode of fracture was found to be quasi-cleavage with more cleavage facets and less microdimples, as shown in Figure 5e. Figure 5h shows the magnified SEM micrographs of the selected areas in Figure 5b, where fracture mode was found to change from ductile to cleavage at the center of Ti1 sample. The ductile and transition zone were characterized by dimples, while cleavage characterized the brittle fracture zone and cleavage facets can be clearly observed on selected magnified region in Figure 5h.

Local cleavage facets and elongated dimples in the vicinity of delamination as shown in Figure 5d,g. At locations away from the delamination site, the fracture mode changed from cleavage to ductile. Instead of cleavage fracture, delamination indicated dimples of a ductile fracture surface and enhanced impact toughness in the ductile to brittle transition region. In general, the stress triaxiality can be reduced by relaxing the σ_{zz} stress component by the delamination of interfaces that are perpendicular to the normal direction (thickness direction) [8]. The reason delamination can improve impact toughness is that delamination changes the stress state near the crack tip to plane stress from plane strain [25]. It is known that cleavage fracture may occur when the stress at the front of crack tip exceeds the cleavage fracture stress. However, the stress near the crack tip can be reduced by delamination, as a result, instead cleavage fracture with some dimples was observed and the delamination can improve the impact toughness in the ductile to brittle transition region. This is the underlying reason for the absence of macroscopic cleavage characteristics in samples with delamination, while the typical cleavage river patterns and crack initiation sites occurred on the fracture surface without delamination in the lower shelf region as shown in Figures 4a,b and 5a,b.

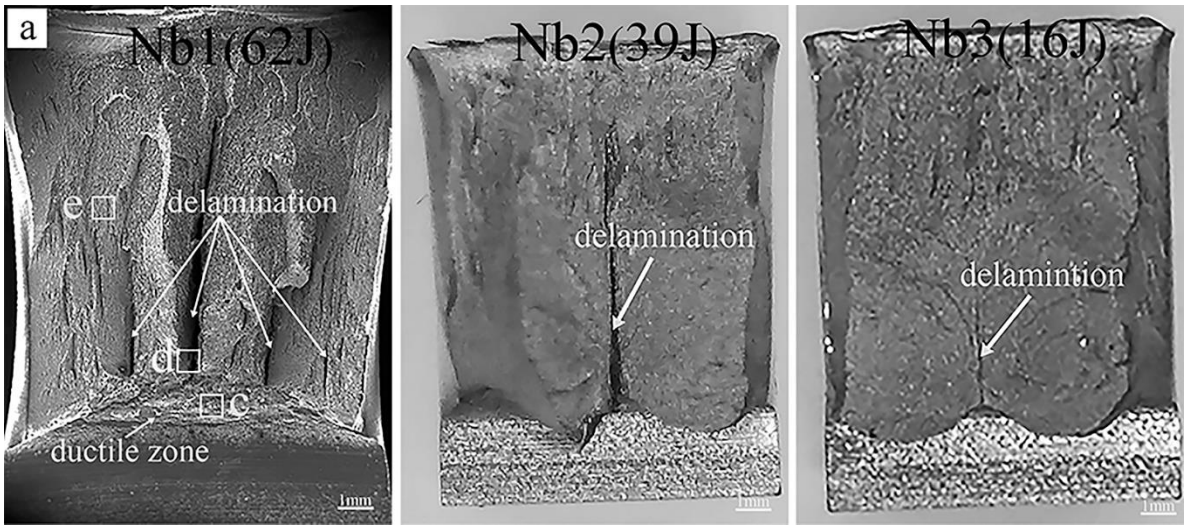

Preprints (www.preprints.org) | NOT PEER-REVIEWED | Posted: 8 July 2019 doi:10.20944/preprints201907.0113.v1

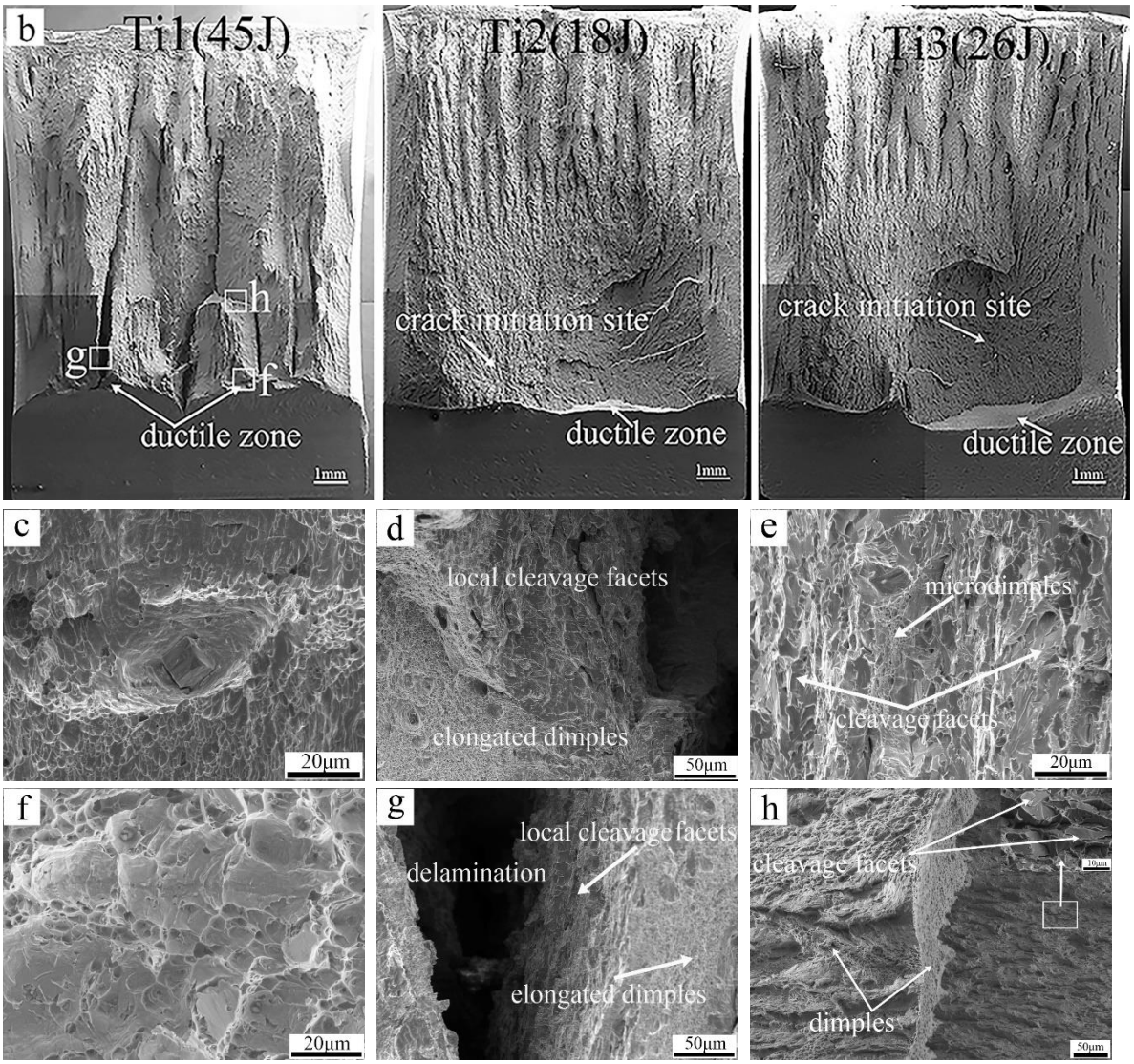

Figure 5. Fracture surface of Charpy impact samples tested at DBTT (**a**) SEM micrographs of fracture surface of Nb-Ti steel with test temperature of -60°C, (**b**) SEM micrographs of fracture surface of Ti steel with test temperature of -20°C, (**c**) (**d**) (**e**) the magnified SEM micrographs of the selected areas marked by 'c', 'd' and 'e' in (a), respectively, (**f**) (**g**) (**h**) the magnified SEM micrographs of the selected areas marked by 'f', 'g' and 'h' in (b), respectively.

It can be seen from Figure 5a that Nb1 sample with higher impact energy because of existing ductile zone and delamination, while Nb2 and Nb3 samples with almost no plastic deformation had a corresponding lower value of impact energy. Nevertheless, the impact energy of Nb2 and Nb3 samples was not particularly low because of the presence of delamination. Moreover, Nb2 sample had a greater impact energy than Nb3 sample because of more severe delamination. Figure 5b indicates that there was little plastic deformation in the three samples. Similarly, Ti1 sample had a higher impact energy than Ti2 and Ti3 samples because of the presence of delamination. The result from fracture analysis indicated that delamination can improve impact toughness in the ductile–brittle transition of the experimental steels.

3.2. Texture analysis

HSLA steels produced by the TMCP may exhibit strong fiber textures, which are related to deformation, recrystallization and phase transformation. In bcc metals, the most important texture

Preprints (www.preprints.org) | NOT PEER-REVIEWED | Posted: 8 July 2019 doi:10.20944/preprints201907.0113.v1

components are found in the φ2=45° section of the Euler space. Figure 6 illustrates the φ2=45° section of the ODFs for the studied steels in the center layer. Some important ideal orientations in rolling are illustrated in Figure 6c to help analyze the texture components. Figure 6a,b illustrate φ2=45° section of the ODFs for Ti and Nb-Ti steels, respectively. It is clear that the intensity of texture in Nb-Ti steel is significantly higher than Ti steel. The deformation textures observed in the mid-plane of the studied steels in the RD-TD plane consisted of (a) α-fiber (φ1 = 0°, Φ = 0° - 90°) or RD ||<110>; (b) γ-fiber (φ1 = 0° - 90°, Φ = 55°) or ND ||<111>; (c) ε-fiber (φ1 = 90°, Φ = 0° - 90°) or TD ||<110>.

The maximum texture intensities of the studied steels were both corresponding to the RD fiber in the orientation space between the {100}<110> and {112}<110> components, and weak {223}<113> texture component is displayed in Figure 6a,b. The RD fiber centered at components from {113}<110> to {112}<110> derived mainly from Cu {112}<111> orientation of the parent austenite rolling texture was responsible for the anisotropy of impact energy [26]. Rotated cube {001}<110> component principally resulting from the cube {001}<100> of the recrystallized austenite texture always made the materials brittle and even expected to cause toughness anisotropy [7]. In contrast, the desirable {332}<113> component which was the transformation product of the Brass {110}<112> in the deformed austenite had much less effect on the anisotropy in mechanical properties [5].

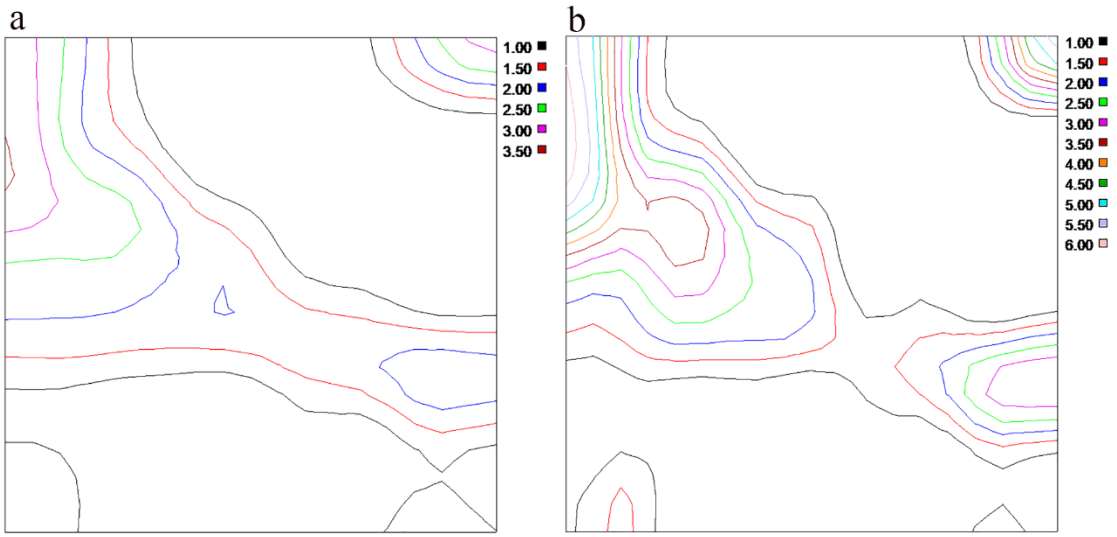

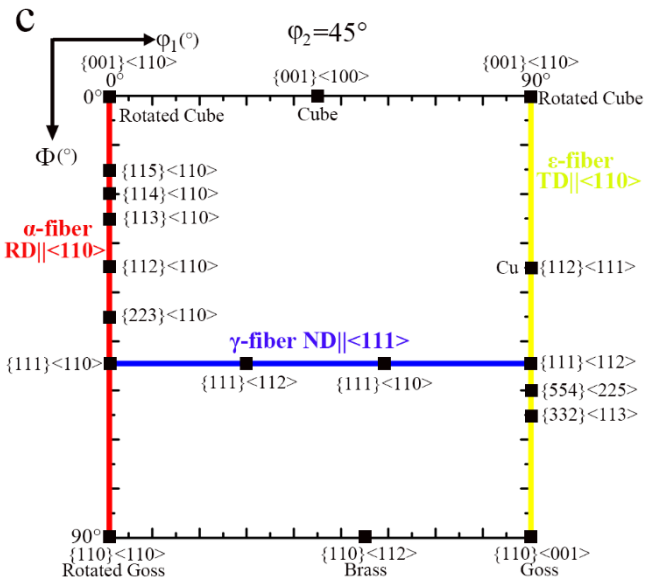

Preprints (www.preprints.org) | NOT PEER-REVIEWED | Posted: 8 July 2019 doi:10.20944/preprints201907.0113.v1

Figure 6. ODFs of experimental steels (**a**) (**b**) ODFs (φ2=45° section) of Ti and Nb-Ti steels, respectively (**c**) φ2=45° section of Euler space showing the positions of the main texture components along with the RD, ND, and TD fibers.

Figure 7 presents details of the α, γ and ε-fibers, which are the most important fibers for hot rolling. With regard to Figure 7a, in the α-fiber, both the steels had the maximum orientation intensity between {100}<110> and {112}<110> and the intensity of these orientations were significantly higher in Nb-Ti steel. It is worth noting from Figure 7b that the γ-fiber contained important recrystallisation components, especially close to {111}<112> and {111}<110>. The γ-fiber texture exhibited different trends in Ti and Nb-Ti steels. The intensity increased gradually from {111}<110> to {111}<112> component in Nb-Ti steel, while a marginal change of intensity occurred in Ti steel. Both the orientation density of ε-fibers in two steels that were centered on {332}<113> and {554}<225> which are transformed components originating from the parent austenite Brass {110}<112> component (Figure 7c).

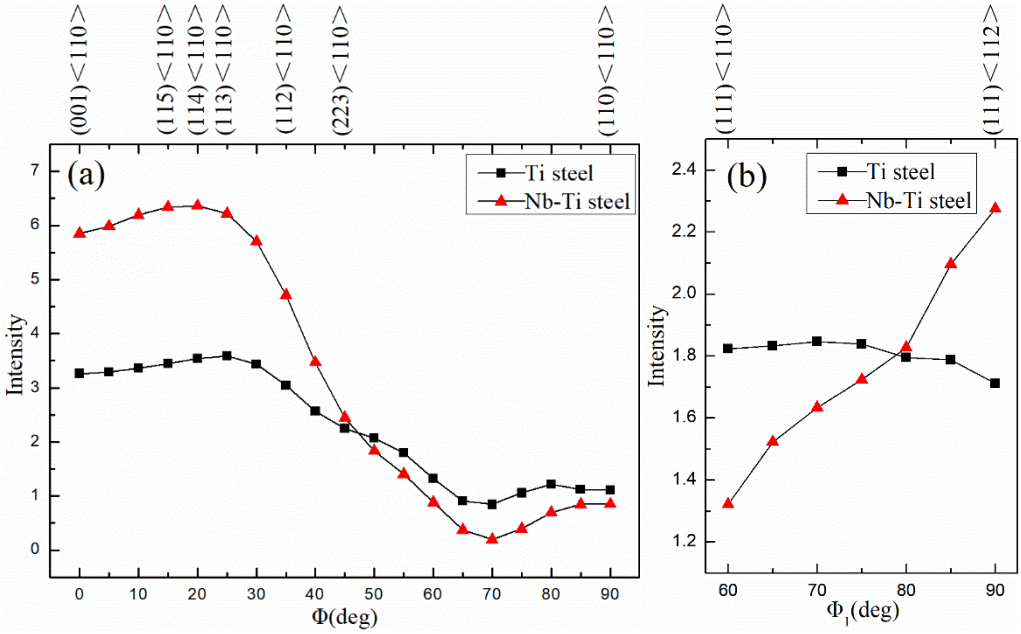

 doi:10.20944/preprints201907.0113.v1

Figure 7. Distribution of principal texture components along (**a**) α-fiber (RD||<110>) (**b**) γ-fiber (ND||<111>) (**c**) ε-fiber (TD||<110>)

In general, the sharpness of the texture depends on the composition of the steel, the rolling process, the initial austenite grain size, and the cooling rate during transformation [27]. Nevertheless, all these factors were similar for both two samples, the sharper texture of Nb-Ti sample is most probably a consequence of a stronger austenite texture because the presence of Nb increases the amount of deformation in the no-recrystallization zone. It is reported that the texture of Nb-microalloyed steels is considerably stronger than carbon steel because precipitation of Nb(C,N) suppresses the recrystallization of γ, thereby leading to a sharp γ rolling texture [22]. The result from texture analysis indicate that a fairly sharp rolling texture can be produced in γ of Nb-Ti steel, which translates into a sharp texture in α products.

3.5. Effect of Texture on delamination

The anisotropy of toughness in steels is usually associated with strong texture, which can cause delamination on impact fracture. As mentioned above, the delamination occurred in the upper and transition region in two steels, and the fracture with delamination occurred at -0 °C, -20 °C, 40 °C C and -60 °C in Nb-Ti samples, while the delamination just occurred at -0 °C and -20 °C in Ti samples. Moreover, after impact test at DBTT of two steels, delamination was found in all three Nb-Ti samples and in only one Ti sample as shown in Figure 5a,b. In summary, it was easier to form delamination in Nb-Ti steels than Ti steels. In general, the delamination is considered to be related to certain texture, ferrite-pearlite microstructure, elongated grains, aligned particles and inclusion banding [13-17]. Pearlite or inclusion banding was not observed and microstructure was similar in two steels. Thus, the different delamination behaviors in two steels are related to the difference in texture.

It is reported that among the transformation texture components found in controlled rolled HSLA steels, the {113}<110> and {112}<110> component causes significant anisotropy in toughness [19,28]. Delamination is associated with the separation of the {001} cleavage planes since {001} planes are the most beneficial for cleavage fracture in bcc metals. Rotated cube {001}<110> component, together with strong {113}<110> and {112}<110>, were expected to cause toughness anisotropy [5,7]. These components in Nb-Ti steel is twice as strong as that of Ti steel, which caused more severe delamination. A fairly sharp fiber texture can be produced in γ by introducing sufficient strain in the austenite non-recrystallization region, which translates into a sharp texture in α-products. However, niobium is an effective microalloying element that retards austenite recrystallization, which is beneficial for accumulating sufficient strain during TMCP and consequent formation of sharp fiber texture. The result of texture and impact fracture analysis indicated that delamination was easier in Nb-Ti samples because of stronger {001}<110>, {113}<110> and {112}<110> texture.

4. Conclusions

1. The representative microstructure of Ti and Nb-Ti steels consisted of ferrite and bainite. Compared with Ti steel, Nb-Ti steel exhibited a microstructure with finer ferrite and more bainite. There is insignificant change in tensile properties, but impact toughness was greater in Nb-Ti steel compared with Ti steel.

2. The typical cleavage river patterns occurred on the fracture surface without delamination, while the macroscopic cleavage characteristics were not observed on delaminated fracture surface,

instead cleavage fracture with some dimples. The study suggests that fracture of delamination in the ductile-brittle transition zone may also representative of high toughness.

3. Compared to Ti steel, more severe delamination occurred in Nb-Ti samples and is attributed to stronger α-fiber (RD ||<110>) texture, especially {001}<110>, {113}<110> and {112}<110> texture.

Author Contributions: All the authors contributed to this research work: Writing—review and editing, M.Y. S. and R.D.K. M; Writing—original draft preparation, M.Y. S.; Conceptualization, X.M. W.; Formal analysis, M.Y. S and X.M. W.; Data curation, X.M W. and M.Y. S..

Funding: This research was funded by the national key research and development plan of China (2017YFB0304700).

Conflicts of Interest: The authors declare no conflict of interest.

References

1. Isasti, N.; Badiola, D.J.; Taheri, M.L.; Uranga, P. Microstructural Features Controlling Mechanical Properties in Nb-Mo Microalloyed Steels. Part II: Impact Toughness. *Metall. Mater. Trans. A* **2014**, *45*, 4972-4982.
2. Li, Z.; Wu, D.; Zhao, X.M.; Yu, H.H.; Luo, L. Influence of rolling and cooling conditions on the mechanical properties of low-carbon cold forging steel. *Metall. Res. Technol.* **2015**, *112*, 204.
3. Calvo, J.; Jung, I.H.; Elwazri, A.M.; Bai, D.; Yue, S. Influence of the chemical composition on transformation behaviour of low carbon microalloyed steels. *Mater. Sci. Eng. A* **2009**, *520*, 90-96.
4. Javaheri, V.; Khodaie, N.; Kaijalainen, A.; Porter, D., Effect of niobium and phase transformation temperature on the microstructure and texture of a novel 0.40% C thermomechanically processed steel. *Mater. Charact.* **2018**, *142*, 295-308.
5. Bakshi, D.; Javed, N.; Sasidhar, K.N.; Dhande, T.; Sharma, V.; Mukherjee, M. Effect of microstructure and crystallographic texture on mechanical anisotropy of Ti-Nb microalloyed hot rolled 800 MPa HSLA steel, *Mater. Charact.* **2018**, *136*, 346-357.
6. Chatterjee, S.; Koley, S.; Bakshi, S.D.; Shome, D. Role of crystallographic texture, delamination and constraint on anisotropy in fracture toughness of API X70 line pipe steels, *Mater. Sci. Eng. A* **2017**, *708*, 254-266.
7. Yang, X.L.; Xun, Y.B.; Tan, X.D.; Wu, D. Influences of crystallography and delamination on anisotropy of Charpy impact toughness in API X100 pipeline steel. *Mater. Sci. Eng. A* **2014**, *607*, 53–62.
8. Song, R.; Ponge, D.; Raabe, D. Mechanical properties of an ultrafine grained C–Mn steel processed by warm deformation and annealing. *Acta Mater.* **2005**, *53*, 4881-4892.
9. Min, X.H.; Kimura, Y.; Kimura, T.; Tsuzaki, K. Delamination toughening assisted by phosphorus in medium-carbon low-alloy steels with ultrafine elongated grain structures. *Mater. Sci. Eng. A* **2016,** *649*, 135-145.
10. Song, R.; Ponge, D.; Raabe, D.; Speer, J.G.; Matlock, D.K. Overview of processing, microstructure and mechanical properties of ultrafine grained bcc steels. *Mater. Sci. Eng. A* **2006**, *441*, 1-17.
11. Kimura, Y.; Inoue, T.; Yin, F.; Sitdikov, O.; Tsuzaki, K. Toughening of a 1500 MPa class steel through formation of an ultrafine fibrous grain structure. *Scripta Mater.* **2007**, *57*, 465-468.
12. Shen, X.J.; Tang, S.; Wu, Y.J.; Yang, X.L.; Chen, J.; Liu, Z.Y.; Misra, R.D.K.; Wang, G.D. Evolution of microstructure and crystallographic texture of microalloyed steel during warm rolling in dual phase region and their influence on mechanical properties. *Mater. Sci. Eng. A* **2017**, *685*, 194-204.
13. Shanmugam, P.; Pathak, S.D. Some studies on the impact behavior of banded microalloyed steel. *Eng. Fract. Mech.* **1996**, *53*, 991-1005.
14. Ray, A.; Paul, S.K.; Jha, S. Effect of Inclusions and Microstructural Characteristics on the Mechanical Properties and Fracture Behavior of a High- Strength Low- Alloy Steel. *J. Mater. Eng. Perform.* **1995**, *4*, 679-688.
15. Tsuji, N.; Okuno, S.; Koizumi, Y.; Minamino, Y. Toughness of Ultrafine Grained Ferritic Steels Fabricated by ARB and Annealing Process. Mater. Trans. **2004**, *45*, 2272-2281.
16. Otárola, T.; Hollner, S.; Bonnefois, B.; Anglada, M.; Coudreuse, L.; Mateo, A. Embrittlement of a superduplex stainless steel in the range of 550–700 °C. *Eng. Fail. Anal.* **2005**, *12*, 930-941.
17. Yang, M.; Chao, Y.J.; Li, X.; Tan, J. Splitting in Dual-Phase 590 high strength steel plates: Part I. Mechanisms. *Mater. Sci. Eng. A* **2008**, *497*, 451-461.

18. Miao, C.L.; Shang, C.J.; Zhang, G.D.; Subramanian, S.V. Recrystallization, Precipitation Behaviors, and Refinement of Austenite Grains in High Mn, High Nb Steel. *Metall. Mater. Trans. A* **2012**, *43*, 665-676.
19. Joo, M.S.; Suh, D.W.; Bae, J.H.; Mouriño, N.S.; Petrov, R.; Kestens, L.A.I.; Bhadeshia, H.K.D.H. Experiments to separate the effect of texture on anisotropy of pipeline steel. *Mater. Sci. Eng. A* **2012**, *556*, 601-606.
20. El-Danaf, E.; Baig, M.; Almajid, A.; Alshalfan, W.; Al-Mojil, M.; Al-Shahrani, S. Mechanical, microstructure and texture characterization of API X65 steel. *Mater. Des*. **2013**, *47*, 529-538.
21. Kaijalainen, A.J.; Liimatainen, M.; Kesti, V.; Heikkala, J.; Liimatainen, T.; Porter, D.A. Influence of Composition and Hot Rolling on the Subsurface Microstructure and Bendability of Ultrahigh-Strength Strip. *Metall. Mater. Trans. A* **2016**, *47*, 4175-4188.
22. Jansto, S.G. MicroNiobium Alloy Approach in Medium and High Carbon Steel Bar, Plate and Sheet Products. *Metall. Mater. Trans. B* **2014**, *45*, 438-444.
23. Wang, R.Z.; Mang. H.T. Strengthening mechanism of Nb and Ti complex microalloyed strip steel produced by thin slab casting and direct rolling process. *Acta. Metall. Sin.* **2007**, *43*, 1082-1090.
24. Verdeja, J.I.; Asensio, J.; Pero-Sanz, J.A. Texture, formability, lamellar tearing and HIC susceptibility of ferritic and low-carbon HSLA steels. *Mater. Charact.* **2003**, *50*, 81-86.
25. Ruggieri, C.; Hippert Jr., E. Delamination effects on fracture behavior of a pipeline steel: Anumerical investigation of 3-D crack front fields and constraint. *Int. J. Pres. Ves. Pip.* **2015**, *128*, 18-35.
26. Venkatsurya, P.K.C.; Jia, Z.; Misra, R.D.K.; Mulholland, M.D.; Manohar, M.; Hartmann Jr., J.E. Understanding mechanical property anisotropy in high strength niobium-microalloyed linepipe steels. *Mater. Sci. Eng. A* **2012**, *556*, 194-210.
27. Ray, R.K.; Jonas, J.J. Transformation textures in steels. *ISIJ Int.***1994**, *34*, 927-942.
28. Nafisi, S.; Arafin, M.A.; Collins, L.; Szpunar, J. Texture and mechanical properties of API X100 steel manufactured under various thermomechanical cycles. *Mater. Sci. Eng. A* **2012**, *531*, 2-11.